JOURNAL OF PROPULSION AND POWER
Vol. 14, No. 3, May–June 1998

Stability Behavior of a Shaft–Disk System Subjected to Longitudinal Force

Lien-Wen Chen* and Hong-Cheng Sheu†
National Cheng Kung University, Tainan 70101, Taiwan, Republic of China

The stability behavior of a spinning Timoshenko shaft with an intermediate attached disk subjected to a longitudinal force is analytically studied. The expressions of frequency (whirl speed) equations for hinged–hinged, hinged–clamped, clamped–hinged, and clamped–clamped rotors are given. By using the numerical technique, the critical axial and follower loads are sought. Numerical results reveal that the instability mechanisms are complex. Eight different types of instability mechanisms are presented. The critical load jump is possible when the instability mechanism changes from one to another. Furthermore, in some special cases, the critical longitudinal loads are almost zero; therefore, such a rotor combination is extremely unstable and should be avoided for design purposes.

Nomenclature

A = area of cross section of the shaft
a_i, b_i = coefficients given by Eqs. (21) and (22), respectively
C_i, $\bar{C}_i$ = integration constants
E = Young's modulus
G = shear modulus
h_i = coefficients given by Eq. (26)
I = moment of inertia of the shaft cross section
I_D, I_P = diameter and polar mass moments of inertia of the disk
$\bar{I}_D$ = nondimensional diameter mass moment of inertia of the disk
I_d, I_p = diameter and polar moments of inertia per unit length of the shaft
j = $\sqrt{-1}$
L = length of the shaft
L_1 = distance between the left end and the intermediate disk
M_D, $\bar{M}_D$ = dimensional and nondimensional mass of the disk
m_i = coefficients given by Eqs. (29) and (32)
$o_i x_i y_i z_i$ = inertia reference frames
p, $\bar{p}$ = dimensional and nondimensional longitudinal loads
$\bar{p}_{cr}$ = nondimensional critical longitudinal load
r = slenderness ratio
s = nondimensional parameter given by Eq. (18)
T = kinetic energy of the rotor
t = time
U_i = normal function of u_i
u_i = $v_i + jw_i$
V = strain energy of the rotor
v_i, w_i = translations in y_i and z_i directions, respectively
W = work done by the external force
α_i = coefficients given by Eqs. (29) and (32)
β_i, γ_i = small rotations about y_i and z_i axes
δ_{1i} = Kronecker delta
η = L_1/L
κ = shear coefficient
μ = direction parameter of the longitudinal load
ξ_i = nondimensional length of the shaft
ρ = mass density of the shaft
Ψ_i = normal function of ψ_i
ψ_i = $\gamma_i - j\beta_i$
Ω, $\bar{\Omega}$ = dimensional and nondimensional spin speeds of the rotor
ω, $\bar{\omega}$ = dimensional and nondimensional whirl speeds of the rotor

Superscript
$\cdot$ = differentiation with respect to time t

I. Introduction

THE current trend in the design of modern rotating machinery, particularly turbomachinery, is toward the achievement of higher operating speeds. Therefore, the accurate dynamic analysis of shaft–disk (rotor) systems has become a fundamental aspect of the design of high-speed turbomachines. There have been a number of investigations relating to this field in the past, as indicated by Dimentberg[1] and Rieger.[2] In those published studies, the main aspects of rotor dynamic behavior are the vibration caused by the imbalance forces and different self-excited sources, stability, and torsional dynamics of shaft. However, of the many important forms of dynamic behavior of a rotor system, the most commonly predicted for design purposes are the stability regions.

In addition to torque transmission, shafts subjected to longitudinal force can be found in many rotating machines. This force can be considered as axial (parallel to the axis of the rotor bearings) because of the pressure difference across the rotor disk. However, if the slope of the shaft at the disk position is significant, the reaction of the working medium, which is perpendicular to the disk, cannot be considered as a constant direction force. It should be taken into consideration that this longitudinal load of the rotor is always tangential to the deflected axis of the shaft and that it follows its motion.

The study of stability of elastic systems subjected to nonconservative forces, such as follower forces, has been of great interest in recent years. A main characteristic of such nonconservative systems is that they are mathematically non-self-adjoint. In general, there exist two types of instability mechanisms, divergence and flutter, for these problems. An excellent treatment of nonconservative stability problems of various kinds of structural components can be found in the early books by Bolotin[3] and Ziegler.[4] A comprehensive discussion of this subject with a related list of references can be found in the book by Leipholz.[5] Czolczynski and Marynowski[6] studied the

Received Dec. 7, 1995; revision received Nov. 5, 1997; accepted for publication Jan. 7, 1998.

*Professor, Department of Mechanical Engineering. E-mail: chenlw@mail.ncku.edu.tw.

†Graduate Student, Department of Mechanical Engineering.

stability of the Laval rotor subjected to a longitudinal force acting on the disk. Yun and Lee[7] derived a qualitative stability criterion to gain physical insights into the behavior of a flexural rotor system subjected to nonconservative torque and force.

For the exact solution of a spinning Timoshenko shaft carrying an intermediate disk subjected to longitudinal force, no such work has been previously investigated. The objective of this paper is to carry out the analytical forms of frequency equations of the spinning Timoshenko shaft with an intermediate disk. To obtain a deeper insight into the dynamic behavior of a shaft–disk system, the present shaft mathematical model has taken account of rotary inertia, shear deformation, gyroscopic moments, and their combined effects. The influence of the spin speed and the intermediate disk on instability mechanisms and their corresponding stability bounds is investigated in detail.

II. Mathematical Formulation

A uniform circular shaft of length L, with a thin rigid disk attached at an arbitrary distance from the left end, subjected to a longitudinal compressive load and spinning along its longitudinal axis at a constant speed Ω is illustrated in Fig. 1. The bearings considered in the present study are rigid, so that supported conditions can be modeled as hinged and clamped supports for short and long bearings, respectively. The bearing combinations considered here are short–short, hinged–hinged (H–H); short–long, hinged–clamped (H–C); long–short, clamped–hinged (C–H); and long–long, clamped–clamped (C–C).

The governing differential equations and corresponding boundary and continuity conditions for such an elastic system can be easily achieved by use of the extended Hamilton's principle. The equations of motion and the boundary and continuity conditions are obtained by the relation

$$\int_{t_1}^{t_2} [\delta(T - V) + \delta W]\, dt = 0 \tag{1}$$

where δW is the variational work done by external forces.

In the present study, the rotor is divided into two portions, the left (from the left end to the intermediate disk) and right (from the intermediate disk to the right end) portions. Two sets of inertia reference frames, $o_1x_1y_1z_1$ with origin o_1 at the left end of the rotor and $o_2x_2y_2z_2$ with origin o_2 at the intermediate disk of the rotor, are adopted. It is assumed that the axial motion is small and can be reasonably neglected. Therefore, a typical cross section of the shaft located at a distance x_i from the origin o_i in a deformed state is described by the translations $v_i(x_i, t)$ and $w_i(x_i, t)$ in the y_i and z_i directions and small rotations $\beta_i(x_i, t)$ and $\gamma_i(x_i, t)$ about y_i and z_i axes, where the subscript $i = 1$ and 2 designate, respectively, the left and right portions of the shaft.

Because the disk is considered to be rigid here, only the strain energy caused by the shaft should be taken into consideration. Taking into account the rotatory inertia and shear deformation, the V for a shaft of A and I is given by

$$V = \frac{1}{2}\int_0^{L_1} \left\{ EI\left[\left(\frac{\partial \beta_1}{\partial x_1}\right)^2 + \left(\frac{\partial \gamma_1}{\partial x_1}\right)^2\right] + \kappa GA\left[\left(\frac{\partial v_1}{\partial x_1} - \gamma_1\right)^2 + \left(\frac{\partial w_1}{\partial x_1} + \beta_1\right)^2\right]\right\} dx_1 + \frac{1}{2}\int_0^{L-L_1} \left\{ EI\left[\left(\frac{\partial \beta_2}{\partial x_2}\right)^2 + \left(\frac{\partial \gamma_2}{\partial x_2}\right)^2\right] + \kappa GA\left[\left(\frac{\partial v_2}{\partial x_2} - \gamma_2\right)^2 + \left(\frac{\partial w_2}{\partial x_2} + \beta_2\right)^2\right]\right\} dx_2 \tag{2}$$

Under the assumption of constant spinning speed, the T of the system including both translational and rotational forms is given by[8]

$$T = \frac{1}{2}\int_0^{L_1} \rho[A(\dot v_1^2 + \dot w_1^2) + I_d(\dot\beta_1^2 + \dot\gamma_1^2) - 2\Omega I_p\beta_1\dot\gamma_1 + \Omega^2 I_p]\, dx_1 + \frac{1}{2}\int_0^{L-L_1} \rho[A(\dot v_2^2 + \dot w_2^2) + I_d(\dot\beta_2^2 + \dot\gamma_2^2) - 2\Omega I_p\beta_2\dot\gamma_2 + \Omega^2 I_p]\, dx_2 + \frac{1}{2}[M_D(\dot v_1^2 + \dot w_1^2) + I_D(\dot\beta_1^2 + \dot\gamma_1^2) - 2\Omega I_P\beta_1\dot\gamma_1 + \Omega^2 I_P]\big|_{x_1 = L_1} \tag{3}$$

Note that $I_p = 2I_d$ and $I_d = I$ for the uniform circular shaft cross section, and $I_P \approx 2I_D$ for the thin circular disk.

The only variational work included in this study is a result of the longitudinal force p and can be expressed as

$$\delta W = \int_0^{L_1} p\left[\frac{\partial v_1}{\partial x_1}\,\delta\left(\frac{\partial v_1}{\partial x_1}\right) + \frac{\partial w_1}{\partial x_1}\,\delta\left(\frac{\partial w_1}{\partial x_1}\right)\right] dx_1 + \mu p(\beta_1\delta w_1 - \gamma_1\delta v_1)\big|_{x_1 = L_1} \tag{4}$$

It is noted here that $\mu = 0.0$ corresponds to the purely axial compressive force and $\mu = 1.0$ corresponds to the fully tangential follower force.

Upon substituting Eqs. (2–4) into the extended Hamilton's principle [Eq. (1)], the governing differential equations for the system are obtained as follows:

$$(\kappa GA - \delta_{1i}p)\frac{\partial^2 v_i}{\partial x_i^2} - \kappa GA\frac{\partial \gamma_i}{\partial x_i} - \rho A\ddot v_i = 0 \tag{5}$$

$$(\kappa GA - \delta_{1i}p)\frac{\partial^2 w_i}{\partial x_i^2} + \kappa GA\frac{\partial \beta_i}{\partial x_i} - \rho A\ddot w_i = 0 \tag{6}$$

$$EI\frac{\partial^2 \beta_i}{\partial x_i^2} - \kappa GA\left(\frac{\partial w_i}{\partial x_i} + \beta_i\right) - 2\rho\Omega I\dot\gamma_i - \rho I\ddot\beta_i = 0 \tag{7}$$

$$EI\frac{\partial^2 \gamma_i}{\partial x_i^2} + \kappa GA\left(\frac{\partial v_i}{\partial x_i} - \gamma_i\right) + 2\rho\Omega I\dot\beta_i - \rho I\ddot\gamma_i = 0 \tag{8}$$

The necessary and sufficient boundary and continuity conditions are found as follows:

Hinged end (at $x_1 = 0$ or $x_2 = L - L_1$):

$$v_1(x_1 = 0, t) = 0, \qquad w_1(x_1 = 0, t) = 0$$
$$\left.\frac{\partial \beta_1(x_1, t)}{\partial x_1}\right|_{x_1 = 0} = 0, \qquad \left.\frac{\partial \gamma_1(x_1, t)}{\partial x_1}\right|_{x_1 = 0} = 0 \tag{9}$$

$$v_2(x_2 = L - L_1, t) = 0, \qquad w_2(x_2 = L - L_1, t) = 0$$
$$\left.\frac{\partial \beta_2(x_2, t)}{\partial x_2}\right|_{x_2 = L - L_1} = 0, \qquad \left.\frac{\partial \gamma_2(x_2, t)}{\partial x_2}\right|_{x_2 = L - L_1} = 0 \tag{10}$$

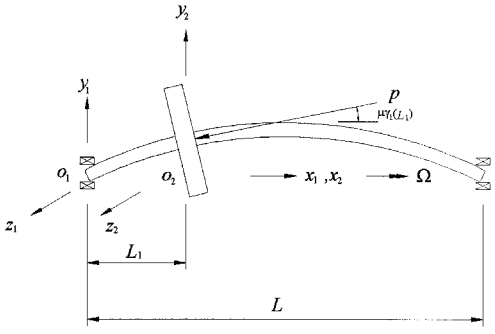

Fig. 1 Spinning rotor and its coordinate systems.

Clamped end (at $x_1 = 0$ or $x_2 = L - L_1$):

$$\begin{aligned} v_1(x_1 = 0, t) &= 0, \qquad w_1(x_1 = 0, t) = 0 \\ \beta_1(x_1 = 0, t) &= 0, \qquad \gamma_1(x_1 = 0, t) = 0 \end{aligned} \tag{11}$$

$$\begin{aligned} v_2(x_2 = L - L_1, t) &= 0, \qquad w_2(x_2 = L - L_1, t) = 0 \\ \beta_2(x_2 = L - L_1, t) &= 0, \qquad \gamma_2(x_2 = L - L_1, t) = 0 \end{aligned} \tag{12}$$

Continuity conditions (across $x_1 = L_1$ and $x_2 = 0$):

$$v_1(x_1 = L_1, t) = v_2(x_2 = 0, t), \quad w_1(x_1 = L_1, t) = w_2(x_2 = 0, t)$$

$$\beta_1(x_1 = L_1, t) = \beta_2(x_2 = 0, t), \quad \gamma_1(x_1 = L_1, t) = \gamma_2(x_2 = 0, t)$$

$$\begin{aligned} &(\kappa GA - p) \frac{\partial v_1(x_1, t)}{\partial x_1}\bigg|_{x_1 = L_1} + M_D \ddot{v}_1(x_1 = L_1, t) \\ &\quad + \mu p \gamma_1(x_1 = L_1, t) = \kappa GA \frac{\partial v_2(x_2, t)}{\partial x_2}\bigg|_{x_2 = 0} \\ &(\kappa GA - p) \frac{\partial w_1(x_1, t)}{\partial x_1}\bigg|_{x_1 = L_1} + M_D \ddot{w}_1(x_1 = L_1, t) \\ &\quad - \mu p \beta_1(x_1 = L_1, t) = \kappa GA \frac{\partial w_2(x_2, t)}{\partial x_2}\bigg|_{x_2 = 0} \\ &EI \frac{\partial \beta_1(x_1, t)}{\partial x_1}\bigg|_{x_1 = L_1} + I_D \ddot{\beta}_1(x_1 = L_1, t) \\ &\quad + 2\Omega I_D \dot{\gamma}_1(x_1 = L_1, t) = EI \frac{\partial \beta_2(x_2, t)}{\partial x_2}\bigg|_{x_2 = 0} \\ &EI \frac{\partial \gamma_1(x_1, t)}{\partial x_1}\bigg|_{x_1 = L_1} + I_D \ddot{\gamma}_1(x_1 = L_1, t) \\ &\quad - 2\Omega I_D \dot{\beta}_1(x_1 = L_1, t) = EI \frac{\partial \gamma_2(x_2, t)}{\partial x_2}\bigg|_{x_2 = 0} \end{aligned} \tag{13}$$

Introducing the complex notations

$$u_i = v_i + j w_i, \qquad \psi_i = \gamma_i - j\beta_i \tag{14}$$

and letting

$$x_i = L\xi_i, \qquad L_1/L = \eta, \qquad u_i = LU_i e^{j\omega t}, \qquad \psi_i = \Psi_i e^{j\omega t} \tag{15}$$

in which ω is the angular frequency.

Omitting the factor $e^{j\omega t}$, Eqs. (5–8) become

$$(1 - \delta_{1i}\bar{p}s^2) \frac{d^2 U_i}{d\xi_i^2} + \bar{\omega}^2 s^2 U_i - \frac{d\Psi_i}{d\xi_i} = 0 \tag{16}$$

$$s^2 \frac{d^2 \Psi_i}{d\xi_i^2} + [\bar{\omega} r^2 s^2 (\bar{\omega} - 2\bar{\Omega}) - 1]\Psi_i + \frac{dU_i}{d\xi_i} = 0 \tag{17}$$

where the nondimensional coefficients are

$$r^2 = \frac{I}{AL^2}, \quad s^2 = \frac{EI}{\kappa GAL^2}, \quad \bar{p} = \frac{pL^2}{EI}, \quad \bar{\omega}^2 = \frac{\rho AL^4 \omega^2}{EI}, \quad \Omega^2 = \frac{\rho AL^4 \Omega^2}{EI} \tag{18}$$

Uncoupling U_i and Ψ_i yields the following equations:

$$\frac{d^4 U_i(\xi_i)}{d\xi_i^4} + 2a_i \frac{d^2 U_i(\xi_i)}{d\xi_i^2} + b_i U_i(\xi_i) = 0 \tag{19}$$

$$\frac{d^4 \Psi_i(\xi_i)}{d\xi_i^4} + 2a_i \frac{d^2 \Psi_i(\xi_i)}{d\xi_i^2} + b_i \Psi_i(\xi_i) = 0 \tag{20}$$

where

$$a_i = [\bar{\omega}^2(r^2 + s^2) - 2\bar{\omega} r^2 \bar{\Omega} - \delta_{1i}\bar{p}(\bar{\omega}^2 r^2 s^2 - 2\bar{\omega} r^2 s^2 \bar{\Omega} - 1)] / [2(1 - \delta_{1i}\bar{p}s^2)] \tag{21}$$

$$b_i = \bar{\omega}^2 [\bar{\omega} r^2 s^2 (\bar{\omega} - 2\bar{\Omega}) - 1] / (1 - \delta_{1i}\bar{p}s^2) \tag{22}$$

The necessary and sufficient boundary and continuity conditions for the system are also expressed in nondimensional complex form as follows:

Hinged end (at $\xi_1 = 0$ or $\xi_2 = 1 - \eta$):

$$\begin{aligned} U_1(\xi_1 = 0) &= 0, \qquad \frac{d\Psi_1}{d\xi_1}\bigg|_{\xi_1 = 0} = 0 \\ U_2(\xi_2 = 1 - \eta) &= 0, \qquad \frac{d\Psi_2}{d\xi_2}\bigg|_{\xi_2 = 1 - \eta} = 0 \end{aligned} \tag{23}$$

Clamped end (at $\xi_1 = 0$ or $\xi_2 = 1 - \eta$):

$$\begin{aligned} U_1(\xi_1 = 0) &= 0, \qquad \Psi_1(\xi_1 = 0) = 0 \\ U_2(\xi_2 = 1 - \eta) &= 0, \qquad \Psi_2(\xi_2 = 1 - \eta) = 0 \end{aligned} \tag{24}$$

Continuity conditions:

$$\begin{aligned} &U_1(\xi_1 = \eta) = U_2(\xi_2 = 0), \qquad \Psi_1(\xi_1 = \eta) = \Psi_2(\xi_2 = 0) \\ &\frac{dU_1}{d\xi_1}\bigg|_{\xi_1 = \eta} - h_1 U_1(\xi_1 = \eta) \\ &\quad + \mu \bar{p} s^2 \Psi_1(\xi_1 = \eta) = \frac{dU_2}{d\xi_2}\bigg|_{\xi_2 = 0} \\ &\qquad \frac{d\Psi_1}{d\xi_1}\bigg|_{\xi_1 = \eta} - h_2 \Psi_1(\xi_1 = \eta) = \frac{d\Psi_2}{d\xi_2}\bigg|_{\xi_2 = 0} \end{aligned} \tag{25}$$

where

$$\bar{M}_D = \frac{M_D}{\rho AL}, \quad \bar{I}_D = \frac{I_D}{\rho AL^3}, \quad h_1 = \frac{\bar{\omega}^2 s^2 \bar{M}_D}{1 - \bar{p}s^2}, \quad h_2 = \bar{\omega} \bar{I}_D (\bar{\omega} - 2\bar{\Omega}) \tag{26}$$

III. Solutions

With the aid of the standard procedure for solving ordinary differential equations, two quartic auxiliary equations are derived. The roots of the auxiliary equations lead to 16 possibilities; however, only two cases are practical and the other 14 cases are of a much higher frequency mode and, hence, of less interest in practical application. Thus, for the sake of saving space, only the two practical cases are presented here.

Case A: suppose that the two auxiliary equations have two real and two pure imaginary roots for each portion of rotor, say, $\pm\alpha_1$, $\pm j\alpha_2$ and $\pm\alpha_3$, $\pm j\alpha_4$, respectively. These happen when $b_1 < 0$ and $b_2 < 0$, and the general solutions of U_i and Ψ_i are then

$$\begin{aligned} U_1(\xi_1) &= C_1 \cosh(\alpha_1 \xi_1) + C_2 \sinh(\alpha_1 \xi_1) \\ &\quad + C_3 \cos(\alpha_2 \xi_1) + C_4 \sin(\alpha_2 \xi_1) \\ \Psi_1(\xi_1) &= m_1 C_1 \sinh(\alpha_1 \xi_1) + m_1 C_2 \cosh(\alpha_1 \xi_1) \\ &\quad - m_2 C_3 \sin(\alpha_2 \xi_1) + m_2 C_4 \cos(\alpha_2 \xi_1) \end{aligned} \tag{27}$$

$$\begin{aligned} U_2(\xi_2) &= C_5 \cosh(\alpha_3 \xi_2) + C_6 \sinh(\alpha_3 \xi_2) \\ &\quad + C_7 \cos(\alpha_4 \xi_2) + C_8 \sin(\alpha_4 \xi_2) \\ \Psi_2(\xi_2) &= m_3 C_5 \sinh(\alpha_3 \xi_2) + m_3 C_6 \cosh(\alpha_3 \xi_2) \\ &\quad - m_4 C_7 \sin(\alpha_4 \xi_2) + m_4 C_8 \cos(\alpha_4 \xi_2) \end{aligned} \tag{28}$$

where

$$\alpha_1 = [-a_1 + \sqrt{a_1^2 - b_1}]^{1/2}, \quad \alpha_2 = [a_1 + \sqrt{a_1^2 - b_1}]^{1/2}$$
$$\alpha_3 = [-a_2 + \sqrt{a_2^2 - b_2}]^{1/2}, \quad \alpha_4 = [a_2 + \sqrt{a_2^2 - b_2}]^{1/2}$$
$$m_1 = [(1 - \bar{p}s^2)\alpha_1^2 + \bar{\omega}^2 s^2]/\alpha_1 \tag{29}$$
$$m_2 = [(1 - \bar{p}s^2)\alpha_2^2 - \bar{\omega}s^2]/\alpha_2$$
$$m_3 = [\alpha_3^2 + \bar{\omega}s^2]/\alpha_3, \quad m_4 = [\alpha_4^2 - \bar{\omega}^2 s^2]/\alpha_4$$

Case B: suppose that the two auxiliary equations have four pure imaginary roots for each portion of rotor, say, $\pm j\alpha_5$, $\pm j\alpha_2$ and $\pm j\alpha_6$, $\pm j\alpha_4$, respectively. These happen when $a_1^2 - b_1 > 0$, $a_1 > 0$, $b_1 > 0$ and $a_2^2 - b_2 > 0$, $a_2 > 0$, $b_2 > 0$, and the general solutions of U_i and Ψ_i are then

$$\begin{aligned} U_1(\xi_1) &= \bar{C}_1 \cos(\alpha_5\xi_1) + \bar{C}_2 \sin(\alpha_5\xi_1) \\ &\quad + \bar{C}_3 \cos(\alpha_2\xi_1) + \bar{C}_4 \sin(\alpha_2\xi_1) \\ \Psi_1(\xi_1) &= -m_5\bar{C}_1 \sin(\alpha_5\xi_1) + m_5\bar{C}_2 \cos(\alpha_5\xi_1) \\ &\quad - m_2\bar{C}_3 \sin(\alpha_2\xi_1) + m_2\bar{C}_4 \cos(\alpha_2\xi_1) \end{aligned} \tag{30}$$

$$\begin{aligned} U_2(\xi_2) &= \bar{C}_5 \cos(\alpha_6\xi_2) + \bar{C}_6 \sin(\alpha_6\xi_2) \\ &\quad + \bar{C}_7 \cos(\alpha_4\xi_2) + \bar{C}_8 \sin(\alpha_4\xi_2) \\ \Psi_2(\xi_2) &= -m_6\bar{C}_5 \sin(\alpha_6\xi_2) + m_6\bar{C}_6 \cos(\alpha_6\xi_2) \\ &\quad -m_4\bar{C}_7 \sin(\alpha_4\xi_2) + m_4\bar{C}_8 \cos(\alpha_2\xi_4) \end{aligned} \tag{31}$$

where

$$\alpha_5 = [a_1 - \sqrt{a_1^2 - b_1}]^{1/2}, \quad \alpha_6 = [a_2 - \sqrt{a_2^2 - b_2}]^{1/2}$$
$$m_5 = [(1 - \bar{p}s^2)\alpha_5^2 - \bar{\omega}^2 s^2]/\alpha_5, \quad m_6 = [\alpha_6^2 - \bar{\omega}^2 s^2]/\alpha_6 \tag{32}$$

The application of appropriate boundary and continuity conditions to Eqs. (27) and (28) or Eqs. (30) and (31) yields a set of eight homogeneous linear algebraic equations for each case. After some algebra reductions, the dimensions of the coefficient matrices become 6×6 for both cases. The elements of these coefficient matrices for each case are given in the Appendix. So that the nontrivial solutions may exist, the determinants of coefficient matrices must be equal to zero. These lead to the frequency equation in each case from which the whirl speeds (natural frequencies) can be determined.

IV. Numerical Results and Discussion

Elastic systems subjected to follower forces can have two types of instabilities: 1) divergence (static instability) and 2) flutter (dynamic instability). Divergence occurs when

$$\bar{\omega}_i = \bar{\omega}_j = 0, \qquad (i \neq j), \qquad i, j = 1, 2, 3, \ldots \tag{33}$$

and flutter occurs when

$$\bar{\omega}_i = \bar{\omega}_j \neq 0, \qquad (i \neq j), \qquad i, j = 1, 2, 3, \ldots \tag{34}$$

In general, the system will be referred to as unstable and its load as critical whenever a static or a dynamic instability occurs.

For typical numerical simulations of the system, the basic nondimensional data employed are the same in all discussion cases; namely, $r = 0.08$ and $E/\kappa G = 3$. For a given rotor with r, s, $\bar{M}_D$, $\bar{I}_D$, $\bar{p}$, μ, η, and $\bar{\Omega}$ known, the $\bar{\omega}_i (i = 1, 2, 3, \ldots)$ can be found from the appropriate frequency equations. When a rotor is put into a spinning motion, its at-rest natural frequency (whirl speed) splits into two components: 1) forward and 2) backward precessions. In all of the figures that follow, the positive whirl speed indicates the forward precession, while the negative whirl speed denotes the backward precession. The first 12 whirl speeds (six forward and six backward modes) are considered to determine the stability bounds. However, there is no proof that the higher modes will not coalesce at an even lower longitudinal load. To minimize length of the present paper, the illustration charts are given only for the H–H rotor.

There exist eight different types of instability mechanisms with the scope of the present study. These instability mechanisms are shown in detail in Fig. 2, which demonstrates the relationships between the $\bar{\omega}$ and $\bar{p}$ for eight different rotor parameters. In Fig. 2, for the sake of convenience, a concise type name is given for each type of instability mechanism. In this scheme, D denotes divergence, F denotes flutter, f and b denote forward and backward precessions, and the digits between two letters represent the coalescent modes. Furthermore, if two instability mechanisms are the same but have a different load-frequency procedure, they will be distinguished by a superscript asterisk. In Fig. 2d, for example, the onset of flutter instability occurs when the two lowest forward whirl speeds coalesce; it is denoted as F12f. However, as shown in Fig. 2h, when the axial force slightly exceeds some value, the first backward whirl speed disappears and immediately changes its natural whirl mode to the forward manner. Because this new emergent forward whirl speed is smaller than the original first forward whirl speed, this new forward whirl speed should be denoted as the first mode and the original first forward whirl speed should now yield to the second forward mode. If the axial load increases continuously and sufficiently, the first two forward whirl speeds move closer and, at some value of $\bar{p}$, coincide with each other; the flutter instability occurs and this type of instability mechanism is called F12f*. The names of the other instability mechanisms can be understood in the same manner.

Figures 3–5 illustrate the influence of the location of the intermediate disk on the critical longitudinal load of H–H rotor with four different intermediate disks, respectively. In each case, four spin speeds, $\bar{\Omega} = 0$, 1.0, 5.0, and 10.0, are considered. It can be observed that the instability boundaries are separated by several significant discontinuities. It is well known that if the critical load jump occurs, the accompanied change of instability mechanism is necessary. However, the converse implication is not always true. For example, when the instability mechanism transits from F12b* through D* to F12f*, the critical load curve is quite smooth without jumping. Generally, the variation of the critical load is fairly smooth for the same instability mechanism. According to the intuition of the stability knowledge, the critical load of the rotor should decrease as η increases; however, this tendency is not always true when the critical load jump occurs because of the change of the instability mechanism. If the acting point of the follower force (nonconservative in nature) is laterally immovable, there is no difference between follower force and the axial load (conservative in nature). Based on this reason, as η approaches 1.0, i.e., the right end support, the critical axial and follower forces are close to each other. However, the critical axial and follower forces are markedly different when the intermediate disk locates away from the right end (see Fig. 4c). Consequently, it can be concluded that neglecting the nonconservative character of the longitudinal load may lead to incorrect results. Furthermore, an interesting observation is that the critical longitudinal load is almost zero in Fig. 5b for $\eta \approx 0.5$. Therefore, the rotor is extremely unstable for such a parameter combination and should be avoided for design purposes.

The dependence of $\bar{p}_{cr}$ on the $\bar{\Omega}$ of the rotor system with four different attached disks is studied next. Here the locations of the intermediate disk are considered to be $\eta = 0.4$ and 0.8, and the results are plotted in Fig. 6 for $\eta = 0.4$ and in Fig. 7 for $\eta = 0.8$. As observed from Fig. 6, the instability mechanism is either F12b* or F12f* for the cases of lower gyroscopic effect, i.e., low $\bar{I}_D$ or $\bar{\Omega}$, and the critical longitudinal load slightly increases with spin speed. When the gyroscopic effect is increased, i.e., high $\bar{I}_D$ or $\bar{\Omega}$, the instability mechanism is F12b regardless of the rotor subjected to follower force or axial

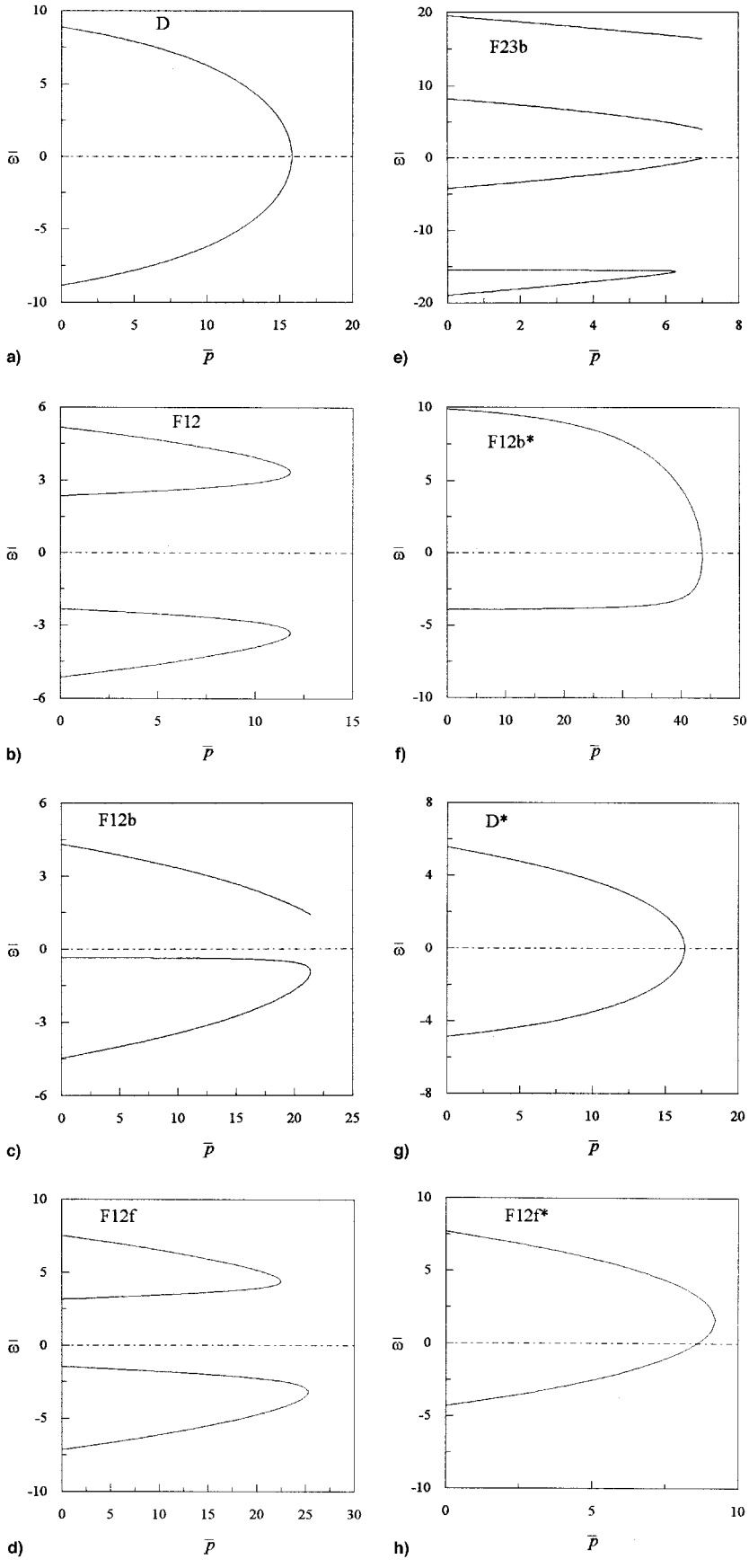

Fig. 2 Load-frequency curves for various types of instability mechanisms: a) $\mu = 0$, $\eta = 0.4$, $\bar{\Omega} = 0$, $\bar{M}_D = 0$, and $\bar{I}_D = 0$; b) $\mu = 1.0$, $\eta = 0.25$, $\bar{\Omega} = 0$, $\bar{M}_D = 5$, and $\bar{I}_D = 0.8$; c) $\mu = 0$, $\eta = 0.25$, $\bar{\Omega} = 10$, $\bar{M}_D = 5$, and $\bar{I}_D = 0.8$; d) $\mu = 1.0$, $\eta = 0.15$, $\bar{\Omega} = 1$, $\bar{M}_D = 5$, and $\bar{I}_D = 0.8$; e) $\mu = 1.0$, $\eta = 0.825$, $\bar{\Omega} = 10$, $\bar{M}_D = 1$, and $\bar{I}_D = 0.032$; f) $\mu = 0$, $\eta = 0.1$, $\bar{\Omega} = 10$, $\bar{M}_D = 1$, and $\bar{I}_D = 0.032$; g) $\mu = 0$, $\eta = 0.3885$, $\bar{\Omega} = 10$, $\bar{M}_D = 1$, and $\bar{I}_D = 0.032$; and h) $\mu = 0$, $\eta = 0.8$, $\bar{\Omega} = 10$, $\bar{M}_D = 1$, and $\bar{I}_D = 0.032$.

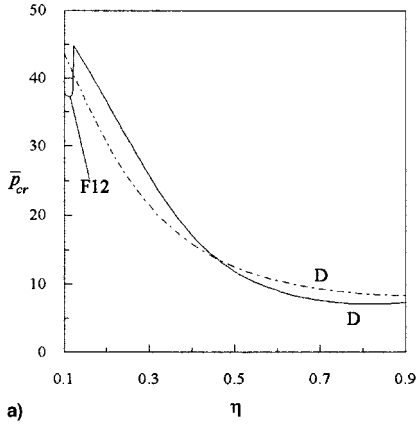

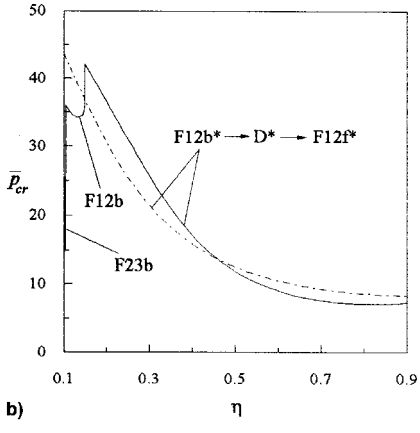

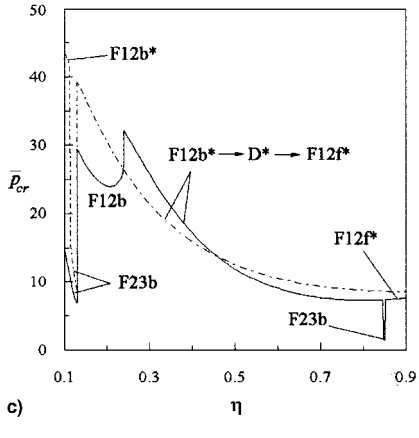

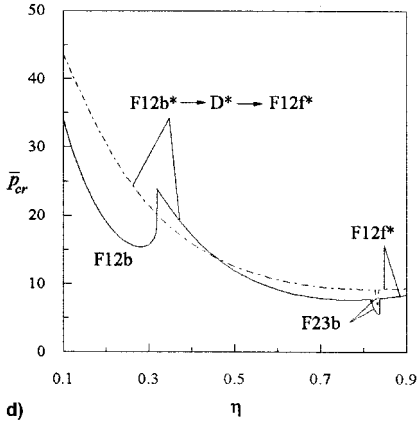

Fig. 3 Stability boundary vs the location of the intermediate disk for $\bar{M}_D = 1.0$, $\bar{I}_D = 0.032$ (·····, axial force; ——, follower force). $\bar{\Omega}$ = a) 0.0, b) 1.0, c) 5.0, and d) 10.0.

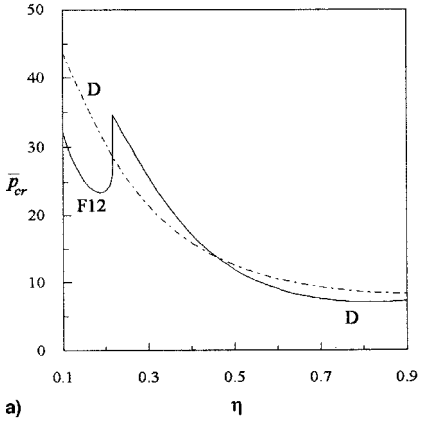

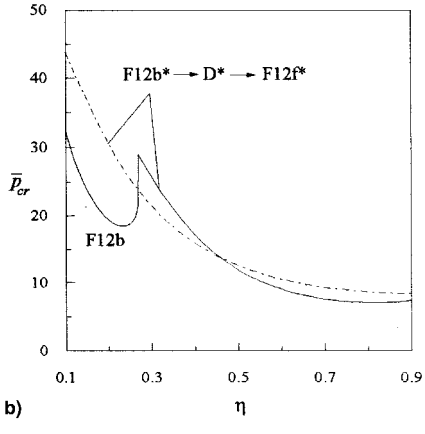

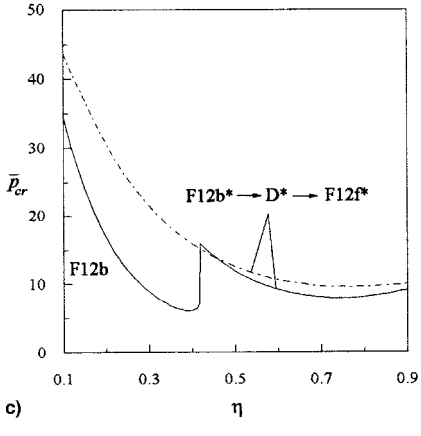

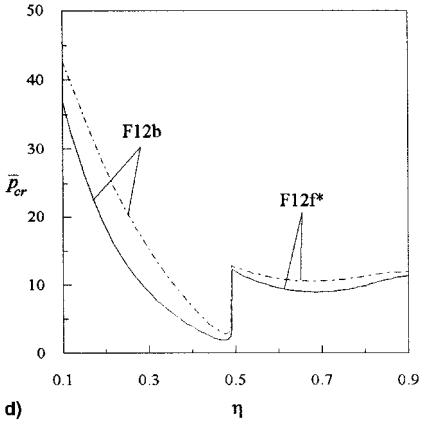

Fig. 4 Stability boundary vs the location of the intermediate disk for $\bar{M}_D = 2.0$, $\bar{I}_D = 0.128$ (·····, axial force; ——, follower force). $\bar{\Omega}$ = a) 0.0, b) 1.0, c) 5.0, and d) 10.0.

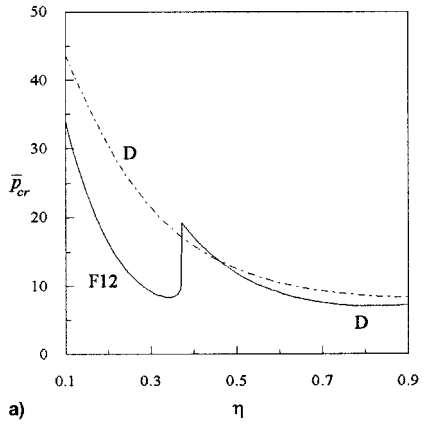

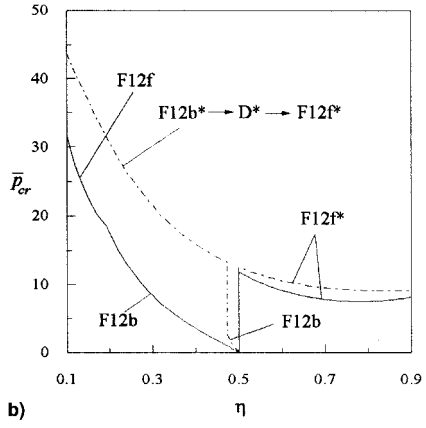

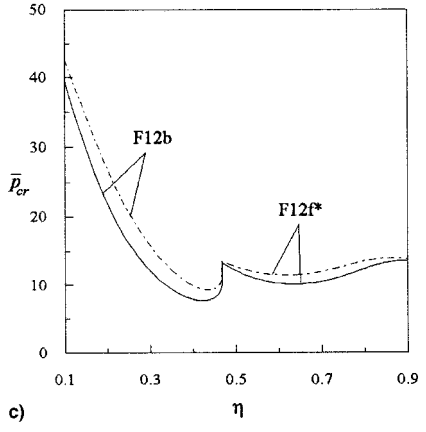

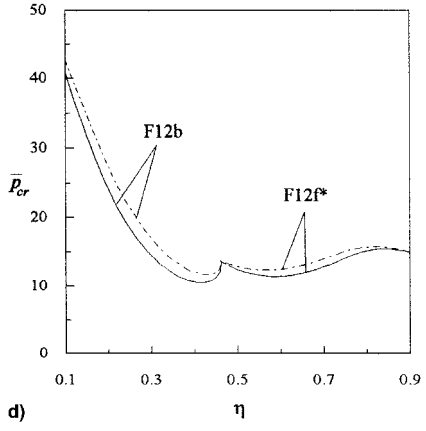

Fig. 5 Stability boundary vs the location of the intermediate disk for $\bar{M}_D = 5.0$, $\bar{I}_D = 0.8$ (-·····, axial force; ——, follower force). $\bar{\Omega}$ = a) 0.0, b) 1.0, c) 5.0, and d) 10.0.

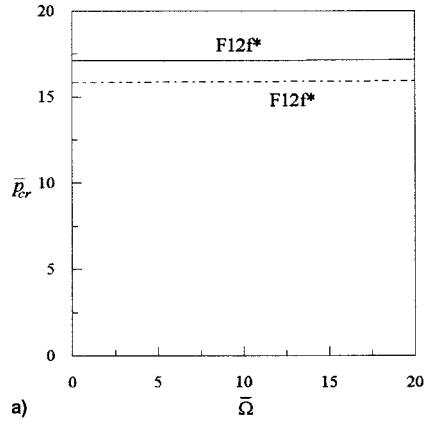

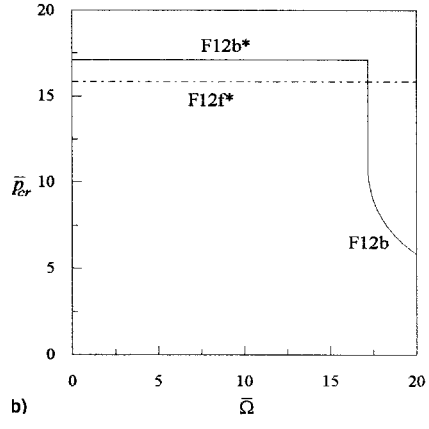

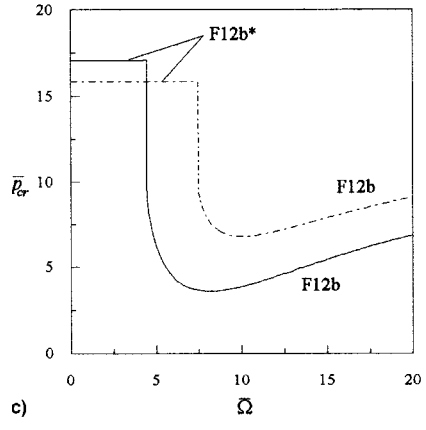

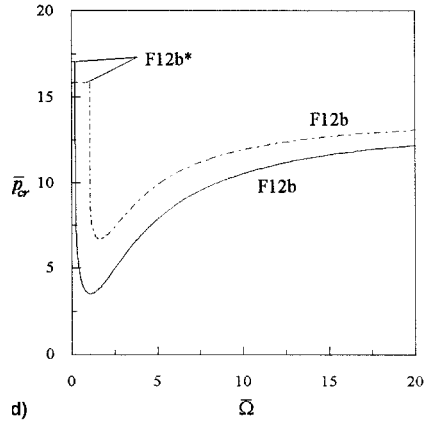

Fig. 6 Stability boundary vs the spinning speed for $\eta = 0.4$ (-·····, axial force; ——, follower force): a) $\bar{M}_D = 0$, $\bar{I}_D = 0$; b) $\bar{M}_D = 1.0$, $\bar{I}_D = 0.032$; c) $\bar{M}_D = 2.0$, $\bar{I}_D = 0.128$; and d) $\bar{M}_D = 5.0$, $\bar{I}_D = 0.8$.

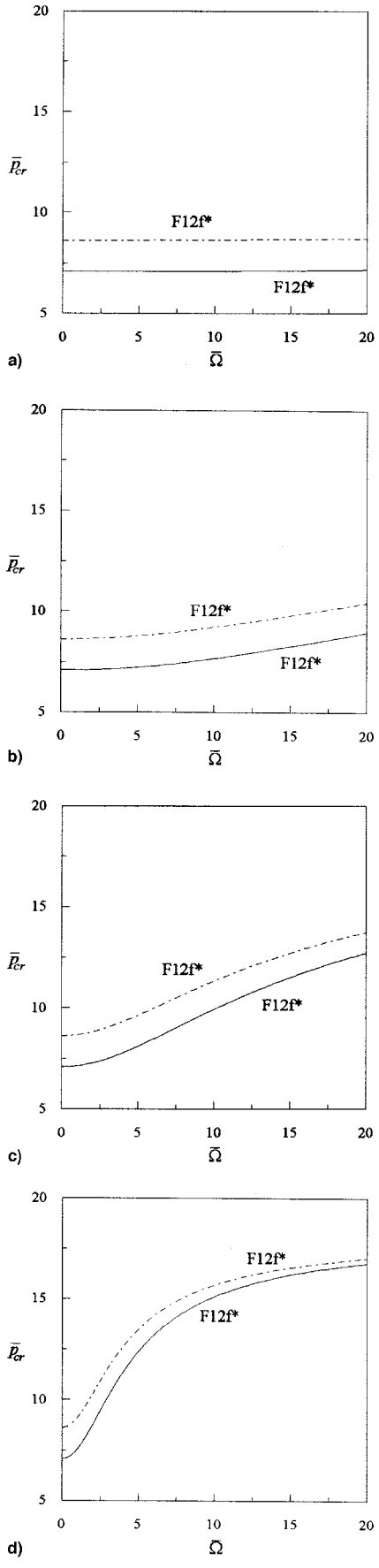

Fig. 7 Stability boundary vs the spinning speed for $\eta = 0.8$ (-·-·-·, axial force; ——, follower force): a) $\bar{M}_D = 0$, $\bar{I}_D = 0$; b) $\bar{M}_D = 1.0$, $\bar{I}_D = 0.032$; c) $\bar{M}_D = 2.0$, $\bar{I}_D = 0.128$; and d) $\bar{M}_D = 5.0$, $\bar{I}_D = 0.8$.

load. After the instability mechanism changes to F12b, the critical longitudinal load initially decreases with the spin speed, and at a spin speed change, it increases. Figure 7 shows that the instability mechanism is F12f*, and the critical longitudinal load increases with the spin speed, particularly for the rotor with a heavy disk (Fig. 7d), its increment is considerable.

V. Conclusions

A stability analysis of a spinning Timoshenko shaft with an attached disk subjected to a longitudinal load is presented. The frequency equations for four types of shaft–disk systems have been derived by the analytical method. From the results of the numerical simulations, the following conclusions can be drawn.

1) Because of the effects of the spin speed, the instability mechanisms of the present elastic system become more complex.

2) The critical load jump is possible when the instability mechanism transits from one to another. Thus, the critical load curve becomes discontinuous and its tendency is hard to predict.

3) In some special cases, the critical longitudinal loads are almost zero; therefore, such parameter combinations of the rotor systems are extremely unstable and should be avoided for design purposes.

4) Neglecting the nonconservative character of the longitudinal load may lead to incorrect results.

5) If the instability mechanism is F12f* or F12b*, the spin speed has a stabilizing effect on the shaft–disk system.

Appendix: Elements of the Matrices for H–H, H–C, C–H, and C–C Rotors

Case A: $b_1 < 0$ and $b_2 < 0$

$$A_{11} = 0, \quad A_{12} = 0, \quad A_{13} = \cosh[\alpha_3(1-\eta)]$$

$$A_{14} = \sinh[\alpha_3(1-\eta)], \quad A_{15} = \cos[\alpha_4(1-\eta)]$$

$$A_{16} = \sin[\alpha_4(1-\eta)], \quad A_{21} = 0, \quad A_{22} = 0$$

$$A_{23} = \begin{cases} m_3\alpha_3 \cosh[\alpha_3(1-\eta)], & \text{for H–H and C–H rotors} \\ m_3 \sinh[\alpha_3(1-\eta)], & \text{for H–C and C–C rotors} \end{cases}$$

$$A_{24} = \begin{cases} m_3\alpha_3 \sinh[\alpha_3(1-\eta)], & \text{for H–H and C–H rotors} \\ m_3 \cosh[\alpha_3(1-\eta)], & \text{for H–C and C–C rotors} \end{cases}$$

$$A_{25} = \begin{cases} -m_4\alpha_4 \cos[\alpha_4(1-\eta)], & \text{for H–H and C–H rotors} \\ -m_4 \sin[\alpha_4(1-\eta)], & \text{for H–C and C–C rotors} \end{cases}$$

$$A_{26} = \begin{cases} -m_4\alpha_4 \sin[\alpha_4(1-\eta)], & \text{for H–H and C–H rotors} \\ m_4 \cos[\alpha_4(1-\eta)], & \text{for H–C and C—C rotors} \end{cases}$$

$$A_{31} = \begin{cases} \sinh(\alpha_1\eta), & \text{for H–H and H–C rotors} \\ \cosh(\alpha_1\eta) - \cos(\alpha_2\eta), & \text{for C–H and C–C rotors} \end{cases}$$

$$A_{32} = \begin{cases} \sin(\alpha_2\eta), & \text{for H–H and H–C rotors} \\ \sinh(\alpha_1\eta) - \dfrac{m_1}{m_2}\sin(\alpha_2\eta), & \text{for C–H and C–C rotors} \end{cases}$$

$$A_{33} = -1, \quad A_{34} = 0, \quad A_{35} = -1, \quad A_{36} = 0$$

$$A_{41} = \begin{cases} m_1 \cosh(\alpha_1\eta), & \text{for H–H and H–C rotors} \\ m_1 \sinh(\alpha_1\eta) + m_2 \sin(\alpha_2\eta), & \text{for C–H and C–C rotors} \end{cases}$$

$$A_{42} = \begin{cases} m_2 \cos(\alpha_2\eta), & \text{for H–H and H–C rotors} \\ m_1[\cosh(\alpha_1\eta) - \cos(\alpha_2\eta)], & \text{for C–H and C–C rotors} \end{cases}$$

$$A_{43} = 0, \qquad A_{44} = -m_3, \qquad A_{45} = 0, \qquad A_{46} = -m_4$$

$$A_{51} = \begin{cases} (\alpha_1 + \mu\bar{p}sm_1)\cosh(\alpha_1\eta) - h_1 \sinh(\alpha_1\eta) \\ \quad \text{for H–H and H–C rotors} \\ (\alpha_1 + \mu\bar{p}s^2m_1)\sinh(\alpha_1\eta) - h_1 \cosh(\alpha_1\eta) \\ \quad + (\alpha_2 + \mu\bar{p}s^2m_2)\sin(\alpha_2\eta) + h_1 \cos(\alpha_2\eta) \\ \quad \text{for C–H and C–C rotors} \end{cases}$$

$$A_{52} = \begin{cases} (\alpha_2 + \mu\bar{p}s^2m_2)\cos(\alpha_2\eta) - h_1 \sin(\alpha_2\eta) \\ \quad \text{for H–H and H–C rotors} \\ (\alpha_1 + \mu\bar{p}s^2m_1)\cosh(\alpha_1\eta) - h_1 \sinh(\alpha_1\eta) \\ \quad - m_1 \left[\left(\dfrac{\alpha_2}{m_2} + \mu\bar{p}s^2 \right) \cos(\alpha_2\eta) - \dfrac{h_1}{m_2} \sin(\alpha_2\eta) \right] \\ \quad \text{for C–H and C–C rotors} \end{cases}$$

$$A_{53} = 0, \qquad A_{54} = -\alpha_3, \qquad A_{55} = 0, \qquad A_{56} = -\alpha_4$$

$$A_{61} = \begin{cases} m_1[\alpha_1 \sinh(\alpha_1\eta) - h_2 \cosh(\alpha_1\eta)] \\ \quad \text{for H–H and H–C rotors} \\ m_1[\alpha_1 \cosh(\alpha_1\eta) - h_2 \sinh(\alpha_1\eta)] \\ \quad + m_2[\alpha_2 \cos(\alpha_2\eta) - h_2 \sin(\alpha_2\eta)] \\ \quad \text{for C–H and C–C rotors} \end{cases}$$

$$A_{62} = \begin{cases} m_2[-\alpha_2 \sin(\alpha_2\eta) - h_2 \cos(\alpha_2\eta)] \\ \quad \text{for H–H and H–C rotors} \\ m_1[\alpha_1 \sinh(\alpha_1\eta) + \alpha_2 \sin(\alpha_2\eta)] \\ \quad - m_1 h_2[\cosh(\alpha_1\eta) - \cos(\alpha_2\eta)] \\ \quad \text{for C–H and C–C rotors} \end{cases}$$

$$A_{63} = -m_3\alpha_3, \qquad A_{64} = 0, \qquad A_{65} = m_4\alpha_4, \qquad A_{66} = 0$$

Case B: $a_1^2 - b_1 > 0$, $b_1 > 0$ and $a_2^2 - b_2 > 0$, $b_2 > 0$

$$\bar{A}_{11} = 0, \quad \bar{A}_{12} = 0, \quad \bar{A}_{13} = \cos[\alpha_6(1-\eta)], \quad \bar{A}_{14} = \sin[\alpha_6(1-\eta)]$$

$$\bar{A}_{15} = \cos[\alpha_4(1-\eta)], \quad \bar{A}_{16} = \sin[\alpha_4(1-\eta)], \quad \bar{A}_{21} = 0, \quad \bar{A}_{22} = 0$$

$$\bar{A}_{23} = \begin{cases} m_6\alpha_6 \cos[\alpha_6(1-\eta)], & \text{for H–H and C–H rotors} \\ m_6 \sin[\alpha_6(1-\eta)], & \text{for H–C and C–C rotors} \end{cases}$$

$$\bar{A}_{24} = \begin{cases} m_6\alpha_6 \sin[\alpha_6(1-\eta)], & \text{for H–H and C–H rotors} \\ -m_6 \cos[\alpha_6(1-\eta)], & \text{for H–C and C–C rotors} \end{cases}$$

$$\bar{A}_{25} = \begin{cases} m_4\alpha_4 \cos[\alpha_4(1-\eta)], & \text{for H–H and C–H rotors} \\ m_4 \sin[\alpha_4(1-\eta)], & \text{for H–C and C–C rotors} \end{cases}$$

$$\bar{A}_{26} = \begin{cases} m_4\alpha_4 \sin[\alpha_4(1-\eta)], & \text{for H–H and C–H rotors} \\ -m_4 \cos[\alpha_4(1-\eta)], & \text{for H–C and C–C rotors} \end{cases}$$

$$\bar{A}_{31} = \begin{cases} \sin(\alpha_5\eta), & \text{for H–H and H–C rotors} \\ \cos(\alpha_5\eta) - \cos(\alpha_2\eta), & \text{for C–H and C–C rotors} \end{cases}$$

$$\bar{A}_{32} = \begin{cases} \sin(\alpha_2\eta), & \text{for H–H and H–C rotors} \\ \sin(\alpha_5\eta) - \dfrac{m_5}{m_2} \sin(\alpha_2\eta), & \text{for C–H and C–C rotors} \end{cases}$$

$$\bar{A}_{33} = -1, \qquad \bar{A}_{34} = 0, \qquad \bar{A}_{35} = -1, \qquad \bar{A}_{36} = 0$$

$$\bar{A}_{41} = \begin{cases} m_5 \cos(\alpha_5\eta), & \text{for H–H and H–C rotors} \\ -m_5 \sin(\alpha_5\eta) + m_2 \sin(\alpha_2\eta), & \text{for C–H and C–C rotors} \end{cases}$$

$$\bar{A}_{42} = \begin{cases} m_2 \cos(\alpha_2\eta), & \text{for H–H and H–C rotors} \\ m_5[\cos(\alpha_5\eta) - \cos(\alpha_2\eta)], & \text{for C–H and C–C rotors} \end{cases}$$

$$\bar{A}_{43} = 0, \qquad \bar{A}_{44} = -m_6, \qquad \bar{A}_{45} = 0, \qquad \bar{A}_{46} = -m_4$$

$$\bar{A}_{51} = \begin{cases} (\alpha_5 + \mu\bar{p}s^2m_5)\cos(\alpha_5\eta) - h_1 \sin(\alpha_5\eta) \\ \quad \text{for H–H and H–C rotors} \\ -(\alpha_5 + \mu\bar{p}s^2m_5)\sin(\alpha_5\eta) - h_1 \cos(\alpha_5\eta) \\ \quad + (\alpha_2 + \mu\bar{p}s^2m_2)\sin(\alpha_2\eta) + h_1 \cos(\alpha_2\eta) \\ \quad \text{for C–H and C–C rotors} \end{cases}$$

$$\bar{A}_{52} = \begin{cases} (\alpha_2 + \mu\bar{p}s^2m_2)\cos(\alpha_2\eta) - h_1 \sin(\alpha_2\eta) \\ \quad \text{for H–H and H–C rotors} \\ (\alpha_5 + \mu\bar{p}s^2m_5)\cos(\alpha_5\eta) - h_1 \sin(\alpha_5\eta) \\ \quad - m_5 \left[\left(\dfrac{\alpha_2}{m_2} + \mu\bar{p}s^2 \right) \cos(\alpha_2\eta) - \dfrac{h_1}{m_2} \sin(\alpha_2\eta) \right] \\ \quad \text{for C–H and C–C rotors} \end{cases}$$

$$\bar{A}_{53} = 0, \qquad \bar{A}_{54} = -\alpha_6, \qquad \bar{A}_{55} = 0, \qquad \bar{A}_{56} = -\alpha_4$$

$$\bar{A}_{61} = \begin{cases} m_5[\alpha_5 \sin(\alpha_5\eta) + h_2 \cos(\alpha_5\eta)], \\ \quad \text{for H–H and H–C rotors} \\ m_5[\alpha_5 \cos(\alpha_5\eta) - h_2 \sin(\alpha_5\eta)] \\ \quad - m_2[\alpha_2 \cos(\alpha_2\eta) - h_2 \sin(\alpha_2\eta)] \\ \quad \text{for C–H and C–C rotors} \end{cases}$$

$$\bar{A}_{62} = \begin{cases} m_2[\alpha_2 \sin(\alpha_2\eta) + h_2 \cos(\alpha_2\eta)], \\ \quad \text{for H–H and H–C rotors} \\ m_5[\alpha_5 \sin(\alpha_5\eta) - \alpha_2 \sin(\alpha_2\eta)] \\ \quad + m_5 h_2[\cos(\alpha_5\eta) - \cos(\alpha_2\eta)] \\ \quad \text{for C–H and C–C rotors} \end{cases}$$

$$\bar{A}_{63} = -m_6\alpha_6, \quad \bar{A}_{64} = 0, \quad \bar{A}_{65} = -m_4\alpha_4, \quad \bar{A}_{66} = 0$$

Acknowledgment

This study was supported by the National Science Council, Taiwan, Republic of China, through Grant NSC85-2212-E-006-037.

References

[1]Dimentberg, F. M., *Flexural Vibrations of Rotating Shafts*, Butterworths, London, 1961.

[2]Rieger, N. F., "Rotor-bearing Dynamics—State-of-the-Art," *Mechanism and Machine Theory*, Vol. 12, 1977, pp. 261–270.

[3]Bolotin, V. V., *Nonconservative Problems of the Theory of Elastic Stability*, Pergamon, New York, 1963.

[4]Ziegler, H., *Principles of Structural Stability*, 2nd ed., Birhäuser, Boston, MA, 1977.

[5]Leipholz, H., *Stability of Elastic Systems*, Sijhoff and Noordhoff, Alphen aan den Rijn, The Netherlands, 1980.

[6]Czolczynski, K., and Marynowski, K. P., "Instabilities of the Elastically Supported Laval Rotor Subjected to a Longitudinal Force," *Journal of Sound and Vibration*, Vol. 154, No. 2, 1992, pp. 281–288.

[7]Yun, J. S., and Lee, C. W., "Dynamic Analysis of Flexible Rotors Subjected to Torque and Force," *Proceedings of the 14th Biennial Conference on Mechanical Vibration and Noise* (Albuquerque, NM), American Society of Mechanical Engineering, New York, 1993, pp. 331–338.

[8]Nelson, H. D., "A Finite Rotating Shaft Element Using Timoshenko Beam Theory," *Journal of Mechanical Design*, Vol. 102, No. 4, 1980, pp. 793–803.